Climate dynamics manuscript No.
(will be inserted by the editor)

Robustness and drivers of the Northern Hemisphere extratropical atmospheric circulation response to a CO_2-induced warming in CNRM-CM6-1

Thomas Oudar · Julien Cattiaux · Hervé Douville · Olivier Geoffroy · David Saint-Martin · Romain Roehrig

Received: date / Accepted: date

Abstract Understanding the mid-latitude atmospheric circulation response to CO_2 forcing is challenging and complex due to the strong internal variability and the multiple potential CO_2-induced effects. While a significant poleward shift of the jet is projected in summer, changes remain uncertain in winter. In this study, we investigate the boreal winter extratropical jet response to an abrupt quadrupling of atmospheric CO_2 in the CMIP6-generation global climate model CNRM-CM6-1. First, we show that the model performs better than the former generation CNRM-CM5 model in representing the atmospheric dynamics in the northern extratropics. Then, when atmospheric CO_2 is quadrupled, CNRM-CM6-1 exhibits a strengthening and upward shift of the jet. A poleward shift is identified and robust in the Pacific in boreal winter. In the Atlantic, the jet response rather exhibits a squeezing, especially at the eastern part of the basin. It is found that changes are more robust across the Northern Hemisphere in early-winter than in late-winter season. Finally, the circulation response is broken down into individual contributions of various drivers. The uniform global mean component of the SST warming

Thomas Oudar
Centre National de Recherches Météorologiques, Université de Toulouse, Météo France, CNRS
42 Avenue Gaspard Coriolis, 31057 Toulouse
Tel.: +335.61.07.94.71
E-mail: thomas.oudar@meteo.fr

is found to explain most of the total atmospheric response to a quadrupling of CO_2, with relatively smaller contributions from faster CO_2 effects, the SST pattern change and the Arctic sea ice decline. The cloud radiative effect contribution is also assessed and found to be rather weak in the CNRM-CM6-1 model. This study highlights that long experiments are required to isolate the wintertime circulation response from the internal variability, and that idealized experimental setups are helpful to disentangle the physical drivers.

Keywords Mid-latitude dynamics · Jet position · Eady growth rate · CO_2 increase · CNRM-CM6-1

1 Introduction

Understanding the response of the large-scale mid-latitude atmospheric circulation to global warming is fundamental as it is the main driver of surface weather for many densely populated regions. For instance, a modification in the speed and/or position of the tropospheric jet which traditionally embeds baroclinic instabilities is likely to affect precipitation patterns and storm trajectories (e.g., Vallis et al, 2015).

In response to an increase in atmospheric greenhouse gases (GHG) concentrations, the troposphere is expected to warm with maximum warming in the tropical upper-troposphere (Meehl et al, 2007; Santer et al, 2008) and near-surface polar regions especially the Arctic (referred to as Arctic Amplification, Holland and Bitz, 2003; Screen and Simmonds, 2010). In the mean time, the stratosphere is expected to cool globally (Shine et al, 2003). This non-uniform response pattern modifies both horizontal and vertical atmospheric temperature gradients, with potential impacts on the mid-latitude atmospheric baroclinicity (Graff and LaCasce, 2012; Ceppi and Shepherd, 2017). It has been recently emphasized that the Arctic Amplification — which is partly due to the Arctic sea ice loss — leads to a decrease of the meridional temperature gradient in the low-level troposphere and can potentially shift the eddy-driven jet equatorward (Deser et al, 2015; Oudar et al, 2017;

McCusker et al, 2017; Barnes and Simpson, 2017; Screen et al, 2018). This effect opposes to the jet poleward shift induced by the tropical upper-tropospheric warming which enhances the meridional temperature gradient aloft (Oudar et al, 2017; McCusker et al, 2017). The influence of the polar vortex response in the lower stratosphere has also been highlighted as a potential source of uncertainty and non-linearity for the wintertime tropospheric circulation response in the northern extratropics (Zappa and Shepherd, 2017; Manzini et al, 2018).

The overall response to a GHG increase simulated by climate models, such as those participating to the fifth Coupled Models Intercomparison Project (CMIP5), is a poleward shift of the eddy-driven jet, at least on the basis of annual and zonal averages (Barnes and Polvani, 2013; Yin, 2005; Vallis et al, 2015; Peings et al, 2018). This suggests that the effect of the tropical upper-tropospheric warming dominates, and is in line with the latitudinal expansion of both Hadley cells (Seidel et al, 2008) and dry regions (Scheff and Frierson, 2012). It is also associated with a poleward shift of the extratropical storm-tracks (Chang et al, 2012; Harvey et al, 2014), increased storminess over Western Europe (Ulbrich et al, 2008), and changes in the flow waviness and atmospheric blockings that are responsible for surface weather variability and extremes (Cattiaux et al, 2016; Francis and Vavrus, 2012).

However this general response hides strong regional and seasonal features. First, it is more robust in the Southern Hemisphere (Kushner et al, 2001) than in the Northern Hemisphere, where it also differs between Atlantic and Pacific basins (Simpson et al, 2014). Second, in the Northern Hemisphere, it is stronger in fall, spring and summer than in winter (Barnes and Polvani, 2015); for instance in the Atlantic, CMIP5 models project no clear latitudinal displacement of the wintertime jet (Cattiaux and Cassou, 2013), but rather a squeezing of its range of possible trajectories (Peings et al, 2018). This suggests that Arctic Amplification, which is the strongest during boreal winter, can cancel out the effect of the tropical upper-tropospheric warming during this particular season.

In addition, the importance of cloud radiative effects on the extratropical circulation has been pointed out by Ceppi and Hartmann (2015). Cloud feedbacks are thought to be responsible for large uncertainties in many aspects of future climate projections including mid-latitude circulation changes (Bony et al, 2015). Several studies have suggested that the poleward shift of the eddy-driven jet (in annual-zonal mean) could be partly explained by the cloud-radiative effect due to cloud changes (Ceppi and Hartmann, 2016; Ceppi and Shepherd, 2017; Voigt and Shaw, 2016; Li et al, 2019; Voigt et al, 2019). In particular, Li et al (2019); Ceppi and Hartmann (2016); Ceppi and Shepherd (2017) showed that about half of the jet shift is due to the atmospheric cloud radiative heating changes. Moreover, Ceppi et al (2014) found that the jet response in the Southern Hemisphere is influenced by the absorbed shortwave radiation that modifies the surface baroclinicity. However, only a few studies rely on realistic modeling experimental setup (Voigt et al, 2019; Li et al, 2019), while other studies used aqua-planet modeling experiments in which several factors are absent (sea-surface temperature [SST] gradients, sea ice or stationary waves). Among others, Voigt et al (2019) used three global climate models and found that the atmospheric pathway (changes in atmospheric cloud-radiative heating) is robust across those models although the magnitude is different.

In this study, we focus on the response of the wintertime (October to March, ONDJFM) Northern Hemisphere mid-latitude atmospheric circulation to an increase of the CO_2 concentration using a set of idealized experiments performed with the CNRM-CM6-1 model for the CMIP6 exercise (Eyring et al, 2016). Our aim is twofold: (i) evaluate how the representation and sensitivity of the atmospheric circulation has evolved since the previous version of the model (CNRM-CM5), and (ii) disentangle the role of the direct radiative and physiological CO_2 effect from the response and slower effects mediated by the SST increase and Arctic sea ice loss.

Similar decomposition has been performed in previous studies (Deser and Phillips, 2009; Grise and Polvani, 2014; Brayshaw et al, 2008; Staten et al, 2012; Ceppi et al, 2018); for instance, Grise and Polvani (2014) used CMIP5 coupled models and showed that the direct radiative effect of CO_2 is responsible for a weak poleward shift of the mid-latitude atmospheric circulation while the indirect effect associated with the surface warming is the dominant factor to explain the poleward shift. Their results are in agreement with Staten et al (2012). Here we use CNRM-CM6-1 atmosphere-only simulations performed within CFMIP (Cloud Feedbacks Model Intercomparison Project, Webb et al (2017)), that allow us to isolate the contributions of the direct radiative and physiological effects of CO_2, the uniform global mean SST warming, the sea ice loss and the SST pattern anomaly (Chadwick et al, 2017). Besides, additional simulations also included in CFMIP allow to investigate the role of cloud radiative effects; here it is evaluated through switching off the cloud radiative effects in the longwave radiation code (see Webb et al, 2017, for more information).

The paper is structured as follows. First, the CNRM-CM6-1 model and the different experiments and metrics are described in Section 2. An evaluation of progress made in the simulation of the mid-latitude atmospheric circulation simulated between CNRM-CM5.1 and CNRM-CM6-1 is done in Section 3. We then assess the response to an abrupt increase of CO_2 in coupled simulations and show that it can be reproduced in atmosphere-only simulations (Section 4). Then, the seasonality and robustness of the response are investigated and we find that robust changes are found in OND rather than in JFM. Thus, Section 5 describes the decomposition of the total response into different effects using atmosphere-only simulations performed under CFMIP for OND season. Among others, contributions of the uniform SST warming, the direct radiative effect of CO_2 and the SST pattern change are investigated. We discuss the results and the role of clouds in the resposne to a uniform SST warming in Section 6. Finally, we conclude in Section 7.

2 Methodology

2.1 Model description

In this study we use the coupled atmosphere-ocean general circulation model (AOGCM) CNRM-CM6-1, recently developed jointly by CNRM (Centre National de Recherches Météorologiques) and CERFACS (Centre Européen de Recherche et de Formation Avançée en Calcul Scientifique) (Voldoire et al, 2019). CNRM-CM6-1 includes the atmospheric model ARPEGE-Climat version 6.3 at a horizontal resolution of 1.4° and with 91 vertical levels (31 vertical levels in the previous version CNRM-CM5). It consists of a almost fully revisited physics package compared to ARPEGE-Climat version 5.1. The surface component is the SURFEX module, which is coupled to ARPEGE-Climat and includes three surface types for land, lakes and ocean. Land surface is treated by the new ISBA-CTRIP coupled system (Decharme et al, 2018). The ocean component of CNRM-CM6-1 is NEMO version 3.6 (Madec et al, 2017), which is run on the eORCA1 horizontal grid. The oceanic resolution is 1° with 75 vertical levels. The sea ice model GELATO version 6 (Voldoire et al, 2013; Chevallier et al, 2013) is embedded in NEMO. The coupler used is OASIS3-MCT (Craig et al, 2017). More details of the models components and an evaluation of the CMIP6 DECK experiments can be found in Voldoire et al (2019).

2.2 Experiments

The evaluation of the CNRM-CM6-1 model (Section 3) is performed using the 10-member `historical` coupled ocean-atmosphere experiment and the 10-member `amip` atmosphere-only experiment (Table 1). The reference dataset is the ERA-Interim reanalysis (Dee et al, 2011) and the reference period is 1979–2014 (36 years). We also use the corresponding experiments from the CNRM-CM5 version, for which we extend the `historical` simulation (originally 1979–2005) with the `rcp85` simulation over 2006–2014.

The mid-latitude atmospheric circulation response to CO_2 forcing is evaluated and analyzed using coupled and time-slice atmosphere-only simulations performed with the CNRM-CM6-1 model for the DECK (Diagnostic, Evaluation and Characterization of Klima, Eyring et al (2016)) and CFMIP (Webb et al, 2017) exercises of CMIP6. The total response to an increase of CO_2 (Section 4) is calculated using the difference between a simulation in which CO_2 is abruptly quadrupled (`abrupt-4xCO2`, C4C) and a control simulation with pre-industrial GHG levels (`piControl`, CPI). Those two experiments have been run over 1500 years with CNRM-CM6-1, which allows to properly isolate the forced response from the internal variability. We also use the same experiments performed with CNRM-CM5 in order to compare the sensitivity of the two model versions.

Two time-slice atmosphere-only experiments forced with SST can be used to evaluate whether or not the total response seen in a coupled model can be reproduced using the AGCM (Atmospheric General Circulation Model) configuration: `piSST` (API) and `a4SSTice-4xCO2` (A4C). In the CFMIP protocol, those simulations use prescribed CO_2 concentrations as well as monthly and annually varying SST and sea ice concentration taken from the years 111-140 of the CPI and C4C coupled experiments, respectively; for the CNRM-CM6-1 model they have been extended over 360 additional years using SST taken from years 111–500, which is helpful to quantify internal variability.

The total response (A4C minus API) can be broken down (Section 5) into individual contributions of direct CO_2 effect, uniform SST increase, SST pattern anomaly and sea ice decline using four others experiments of 30 years each (Table 1 and Equation 1): `piSST-4xCO2` (ACO2), `piSST-pxK` (AUNI), `a4SST` (ASST), and `a4SSTice` (AICE). `piSST-4xCO2` is the same as `piSST` but with CO_2 quadrupled. `a4SST` is the same as `piSST` but with SSTs taken from years 111-140 of the `abrupt-4xCO2` experiment (sea ice is unchanged). `a4SSTice` is the same as `a4SST` but sea ice is also taken from years 111-140 of the `abrupt-4xCO2` experiment. `piSST-pxK` is the same as `piSST` but with a SST anomaly applied uniformly and corresponding to the difference in global mean SST between `abrupt-4xCO2` and `piControl` experiments. Those experiments are part of the Tier 2 of CFMIP and more information about initial conditions and forcings can be found in Webb et al (2017). The decomposition can then be written as:

$$\underbrace{A4C - API}_{total} = \underbrace{A4C - AICE}_{direct\ CO2} + \underbrace{AICE - ASST}_{sea\ ice} + \underbrace{ASST - AUNI}_{SST\ pattern} + \underbrace{AUNI - API}_{uniform\ SST} \tag{1}$$

Note that the direct CO_2 effect can also be calculated as the difference ACO2 minus API (in which the SSTs are taken from the control experiment). The linearity of the CO_2 effect has thus been briefly investigated, but we have not found significant differences between the two methods to estimate this effect.

As these additional simulations have been performed over 30 years only, we consider years 111–140 of API and A4C for consistency when computing the decomposition.

Finally, in addition to these simulations, AMIP-type simulations performed over the period 1979-2014 are used to evaluate the cloud feedback on the atmospheric circulation (Table 1). The reference is the `amip` simulation, i.e. the atmosphere-only experiment prescribed with observed 1979–2014 SST. The perturbed climate is the `amip-p4K` simulation in which the SST are uniformly increased by 4 K. Two parallel experiments have been run within CFMIP with the cloud radiative effect switched off in the long-wave radiation code: `amip-lwoff` and `amip-p4K-lwoff`. The long-wave cloud feedback is determined as follows: (i) the response to a 4K-warming is computed with and without cloud radiadive effect (`amip-p4K` minus `amip` noted “ON” and `amip-p4K-lwoff` minus `amip-lwoff` noted “OFF”), and (ii) the difference ON minus OFF is calculated. Again, more information on how those experiments were performed can be found in Webb et al (2017, see their Table 2).

2.3 Metrics

We choose to use a limited number of commonly used metrics to evaluate the representation and sensitivity of the atmospheric circulation in CNRM-CM6-1. We thus only focus on an index of maximum wind position, which characterizes the location of the eddy-driven jet, and the Eady Growth Rate (EGR) parameter (Lindzen and Farrell, 1980), which is a measure of baroclinicity and gives the potential energy available for the growth of extratropical storms. Both metrics are detailed below. Note that a North-Atlantic Oscillation index is used in the CNRM-CM6-1 reference paper (Voldoire et al, 2019).

2.3.1 Maximum wind position

In the mid-latitudes, the latitudinal position of the jet stream is crucial as it determines the trajectories for synoptic systems that travel across the Pacific and the Atlantic (e.g. wintertime storms). This circulation diagnostic has thus received particular attention in previous studies (Woollings et al, 2010; Barnes and Polvani, 2013). The authors usually localize the latitude of the eddy-driven jet separately between the Pacific and the Atlantic, where it is well established, rather than continuously across the globe. Here we consider three different regions:

- Central Atlantic: 60–0°W, 15–75°N;
- East Atlantic: 0–30°E, 15–75°N;
- Pacific: 100–260°E, 15–75°N.

Our Central Atlantic domain corresponds to the single Atlantic domain used in Woollings et al (2010) and Barnes and Polvani (2013), but here we find important to also consider an East Atlantic region, as it exhibits a different behavior (shown later in the paper). However, as the existence of a well established low-level jet is questionable over this region, we will here refer to this diagnostic as “maximum wind position” rather than “eddy-driven jet position”.

Similarly to Woollings et al (2010), the maximum wind position is then identified as follows:

1. The zonal wind is averaged over the levels 850 and 700 hPa.
2. A zonal average is applied over the region of interest (Central Atlantic, East Atlantic and North Pacific).
3. A first guess of the maximum wind position is identified as the latitude at which the wind speed is maximum.
4. Finally, a parabola is fitted on the zonal wind speed taken over a 11-gridpoint window centered on the first guess, and the maximum wind position corresponds to the maximum of the parabola. This step allows to smooth the zonal wind speed around its maximum.

2.3.2 Eady Growth Rate

The EGR is a measure of baroclinicity of the flow and is a function of the vertical wind shear (linked to the meridional temperature gradient via the thermal wind balance) and the Brunt-Vaisala frequency (measure of static stability and related to the vertical gradient of temperature). The EGR is given by the formula:

$$\sigma = 0.31 \frac{f}{N} \frac{\partial u}{\partial z} \tag{2}$$

where N is the Brunt-Vaisala frequency (in day^{-1}, θ the potential temperature (in K) and $\frac{\partial u}{\partial z}$ the vertical wind shear. Following the thermal wind relationship, this formula can be written:

$$\sigma = 0.31 g \frac{1}{N} \frac{1}{\theta} \frac{\partial \theta}{\partial y} \tag{3}$$

The EGR and maximum wind position are determined using monthly outputs, as daily outputs were not available for all simulations. It is worth mentioning that using monthly outputs generates biases in the calculation of the EGR (Simmonds and Lim, 2009), but we have verified that the pattern of the response is not changed with daily outputs when available (not shown).

3 Model evaluation

In this section, we evaluate the representation of wintertime mid-latitude atmospheric circulation by the two versions of the CNRM-CM models. Figure 1 first shows the ONDJFM 850 hPa zonal wind biases for AOGCM and AGCM configurations of CNRM-CM5 and CNRM-CM6-1. For both versions of the model, there are notable similarities between AOGCM and AGCM biases, suggesting that circulation biases mostly arise from the atmospheric model. For both configurations, the global bias is reduced in the new version (CNRM-CM6-1), as highlighted by root-mean squared errors (indicated on the top right of each panel); this suggests a general improvement in the representation of the mean flow. A common characteristic to climate models, including CNRM-CM, is that the mid-latitude flow is too zonal, especially in the North Atlantic region. Both model versions indeed exhibit negative (positive) biases north (south) of the maximum wind climatology. This regional bias is also slightly reduced in the new version, particularly for the AOGCM (Figure 1b,d). In the Pacific, the bias pattern is more complex, with marked differences between AOGCM and AGCM configurations. The AOGCM has a strong positive bias in CNRM-CM5 which is largely reduced in CNRM-CM6-1 at the exception of the western edge of the basin (Figure 1b,d). The AGCM rather exhibits a tripolar bias pattern (Figure 1a,c). This bias is also weaker in CNRM-CM6-1.

To further investigate the representation of the mean atmospheric circulation, Figure 2 shows distributions of the maximum wind position for the different domains defined in Section 2. Over the Central Atlantic, the maximum wind position is equatorly biased in CNRM-CM models compared to ERA-Interim, albeit with a weaker bias in CNRM-CM6-1 (Figure 2a). This is consistent with Figure 1 and the too zonal bias. Over the East Atlantic (Figure 2b), the distribution exhibits a tripolar structure of the maximum wind position in ERA-Interim, that was already highlighted by Woollings et al (2010, 2018). This tripolar structure is captured by CNRM-CM models, and the repartition among the three peaks of the distribution is better represented in CNRM-CM6-1. In the North Pacific (Figure 2c), the maximum wind position is well represented by the CNRM models, with again slight improvements in CNRM-CM6-1 compared to CNRM-CM5. The maximum wind position is also indicated for the AGCM versions in dashed lines and we find consistent results with Figure 1.

The better representation of jet features in CNRM-CM6-1 is associated with a better representation of the EGR. Figure 3 shows the wintertime climatology of the zonal-mean EGR for ERA-Interim, CNRM-CM6-1 and CNRM-CM5. The EGR exhibits maximum in the mid-to-high troposphere between 30°N and 40°N and near the surface between 30°N and 40 °N. The climatology is well represented by the CNRM-CM6-1 model even if the EGR is slightly overestimated near the surface. Nonetheless, improvement are depicted when comparing CNRM-CM6-1 with CNRM-CM5: in the latter, the EGR is overestimated in the mid-to-high troposphere, but is better represented in the low-troposphere than the former. This conclusion is consistent with Voldoire et al (2019), who also pointed out an improvement in the representation of the NAO (North Atlantic Oscillation).

4 Mid-latitude circulation response

4.1 Mean changes in coupled experiments

The aim of this section is to assess the atmospheric circulation response to an abrupt increase in CO_2 in coupled experiments (CPI and C4C) and to compare CNRM-CM6-1 with CNRM-CM5. We first look at the zonal-mean temperature response for CNRM-CM5 and CNRM-CM6-1 (Figure 4a,b). The pattern between the two versions is similar and the correlation is of about 0.96. It exhibits a warming in the troposphere, particularly in the polar lower-troposphere and in the tropical upper-troposphere, as well as a cooling in the stratosphere. This pattern of temperature response to a CO_2 increase is theoretically expected (e.g., Vallis et al, 2015) and classically found in numerical studies (Peings et al, 2018; Deser et al, 2015, among many others). We find greater anomalies in CNRM-CM6-1, indicating a stronger climate sensitivity in this new version of the model. This is in agreement with Voldoire et al (2019) who report an equilibrium climate sensitivity (ECS) of 4.9 K in CNRM-CM6-1 and 3.3 K in CNRM-CM5.

Consistently, the zonal-mean zonal wind anomalies are greater in CNRM-CM6-1 than in CNRM-CM5 (Figure 4d,e), while the pattern is qualitatively similar (correlation coefficient of 0.88). The zonal wind strengthens and shifts upward at around 30°N, and a weakening is observed in higher latitudes in both versions, although the shape is a bit different. CNRM-CM5 does not exhibit any latitudinal shift of the zonal wind while a small poleward shift is observed in CNRM-CM6-1 near the surface between 40°N and 50°N. Regional changes are important in the Northern Hemisphere and Figure 4g,h details the 850 hPa zonal wind response. The two versions of the model agree on the strengthening of the zonal wind over the British Isles, although the magnitude of the change is weaker in CNRM-CM5. Over the Central Atlantic, the two versions differ: CNRM-CM5 shows a weakening while CNRM-CM6-1 exhibit a slight strengthening. The difference might be due to the strong internal variability over this region; this issue will be discussed later in the paper. In the Pacific, both versions agree on the strengthening of the zonal wind, albeit with different spatial patterns. CNRM-CM5 projects a maximum strengthening over the Eastern Pacific while CNRM-CM6-1 projects the highest increase in the Western part, together with a slight poleward shift. These regional discrepancies result in a relatively weak correlation coefficient (0.55) between the two model responses.

4.2 Mean changes in atmosphere-only experiments

Here we explore whether the response seen in the coupled model is reproducible by the AGCM. This is illustrated by comparing panels b and c, e and f, h and i in Figure 4 for the zonal-mean temperature, the zonal-mean zonal wind and the 850 hPa zonal wind, respectively. For these three fields, the responses in CNRM-CM6-1 coupled experiments (CPI and C4C) are well reproduced in the atmosphere-only experiments (API and A4C). The correlations are of about 0.99 for the zonal-mean fields and 0.89 for the 850 hPa zonal wind. Some regional differences are identified, especially over the central Atlantic region in which anomalies are stronger in atmosphere-only than in coupled simulation. As described in Section 2.2, years 111-140 have been used to characterize the response. However, as more years are available for C4C, CPI, A4C and API, it is possible to test the robustness of the pattern observed in Figure 4. In particular, if the response is computed over all years available common between the coupled and AGCM experiments (after removing the first 111 years for the coupled experiments), consistency between the response in coupled and atmosphere-only experiments is found (Figure 5). Thus, it is likely that the response observed in the AGCM experiments (Figure 4i) over the years 111-140 is affected by internal variability. This issue will be discussed in Section 4.4.

4.3 Maximum wind position

Figure 6a,b,c shows the distribution of the maximum wind position in the lower troposphere for the Central Atlantic, East Atlantic and Pacific domains respectively, for both CPI and C4C experiments. The poleward shift in the Pacific (Figure 6c) is robust and consistent with the 850 hPa zonal wind response in Figure 4h. Over the Central Atlantic domain (Figure 6a), no systematic shift of the zonal wind is observed but rather a slight squeezing of the distribution. This squeezing is more pronounced over the East Atlantic (Figure 6b), where the tripolar structure observed in the pre-industrial climate is almost lost when CO_2 is quadrupled. Such a squeezing of the range of jet trajectories was already reported in CMIP5 models by Peings et al (2018). It is also related to the strengthening of the zonal wind over Western Europe (Figure 4i) associated to an increase in storminess over this region found in several studies (Ulbrich et al, 2008; Harvey et al, 2014). Interestingly, similar results are found for the response in AGCM simulations (not shown). This confirms that the response to an abrupt CO_2 increase simulated in coupled experiments is well reproduced by the AGCM model.

4.4 Seasonality of the response

We have shown the response to a CO_2 increase for an extended winter season (ONDJFM). However, changes in mid-latitude dynamics can be uncertain for this season, at least for two reasons: (i) the internal variability is stronger which reduces the signal-to-noise ratio and (ii) a subtle balance between competitive effects is at play (upper-tropospheric tropical warming and surface Arctic amplification). As shown in Barnes and Polvani (2015) from CMIP5 models, other seasons exhibit a more significant and robust poleward shift of the jet position (see their Figure 4). Here we therefore comment jet changes in other seasons.

Figure 7a shows the maximum zonal wind position response to a quadrupling of CO_2 in the coupled model CNRM-CM6-1 (C4C minus CPI) for different regions and seasons (ONDJFM, OND, JFM, AMJ, JAS). Note that over the full period available for the coupled simulations (1500 years), almost all responses are significant (i.e. green dots are filled). The black dots (red when significant) correspond to the response over years 111-140. The response calculated over this subset of years is always of the same sign as the response calculated over the full period. However, changes over this period are not always significant, which raises the question whether 30 years are sufficient to estimate responses of the mid-latitude atmospheric circulation in the CNRM-CM6-1 model. To test the variability of the response if only 30 years are available, we calculated the response in 1000 30-year periods selected randomly in the 1500 years. The response is represented by the small gray (red if the change is significant) cross. A striking result is the lower variability in the response in the Pacific compared to the Atlantic. In the Pacific, the maximum wind position is significantly shifted northward in ONDJFM, OND and JFM (a bit less in JFM), suggesting that the poleward shift is robust in the Pacific in fall and winter. Another important result from this figure is the contrasted responses between OND and JFM seasons: in JFM there is no clear response (especially in the Atlantic) while the maximum wind position response exhibits almost only positive values in OND for each regions. Moreover, in the Atlantic, negative or positive responses can be found when looking at 30 years period in ONDJFM and JFM, meaning that internal variability is strong in the Atlantic region. This issue is discussed in the next section. Although the latitude of the maximum zonal wind is not significantly changed for each region in winter and fall, the zonal wind strengthens significantly for these seasons. Looking at spring and summer seasons, the maximum wind position is shifted northward in the Central Atlantic, whereas no changes are seen in the East Atlantic and in the Pacific (note that the variability of the response is strong in the Pacific for the summer season). In spring and summer, there is a weakening although some uncertainties still remain (Figure 7b). Similar conclusions are drawn for the AGCM experiments (not shown).

4.5 Significance and internal variability

The previous section shows that 30-year periods can be insufficient to isolate the CO_2 response from internal variability. Figure 8 illustrates this issue showing a time series of robustness for the maximum wind position response, for different regions (Central Atlantic, East Atlantic and North Pacific) and for ONDJFM (black curve), JFM (blue curve) and OND (red curve). For each N from 10 to 1500, we randomly select 1000 samples of N years in the 1500 years available for both CPI and C4C simulations and calculate the C4C minus CPI mean difference over each sample. For each duration, we count the number of times when the response is of the same sign of the response found over the full period and significant at the 95% confidence level. It gives an estimation of the power of the statistical test and we consider that robustness is reached at the 50% level (dashed red line on Figure 8). This figure indicates that significance is reached much faster in the Pacific (i.e. with smaller samples) than in the Atlantic, showing the greater importance of internal variability in the Atlantic. Only a dozen of years is needed to find a significant change in ONDJFM and OND in the Pacific and about 100 years for JFM. In the Atlantic (for both East and Central Atlantic regions), approximately 30 years are needed to find significant change in OND but the interpretation is rather different for ONDJFM and JFM seasons. Over the Central Atlantic region in ONDJFM, the internal variability is strong (about 400 years are needed), while only 100 years in JFM are needed to reach robustness. Over the East Atlantic region, more than 300 years are needed to find robust changes in JFM. This result suggests the important role of internal variability in the Atlantic, especially in ONDJFM and JFM season, and that caution is needed when analyzing atmospheric circulation changes in that region, especially from short time-slice experiments.

Zappa et al (2015) investigated the time of emergence of the 850 hPa zonal wind projections in CMIP5 models. They found that the time of emergence was reduced when looking at extended seasonal averages (winter or summer) compared to classics meteorological seasons (DJF for example). Their results somehow contrast with our and reason for that can be that they focus on the detection of a signal over specific regions (Central Europe and North Africa in winter) whereas we are looking if the zonal wind shifts or not. For example, over the East Atlantic region, Figure 8b shows that significance emerges much faster in OND than in ONDJFM, probably because the poleward shift is much more pronounced in OND than in ONDJFM (Figure 7a). However, this analysis does not tell if the signal observed over Western Europe (strengthening of the zonal wind) is significant or not. It has to be noted that the maximum wind position is an integrated metric.

Nevertheless, as robust changes are found for OND, we decide to focus on this season for the rest of the paper and to break down the total circulation response into contributions of various drivers using atmosphere-only simulations performed under the CFMIP protocol. Note that analysis presented hereafter have been performed for the other seasons (not shown).

5 Breakdown of the AGCM response

5.1 Temperature response

Figure 9 shows the breakdown of the total AGCM zonal-mean temperature response for OND season (panel a) into contributions of uniform SST increase, sea ice loss, direct CO_2 effect and SST pattern anomaly, respectively (panels b to e). The two dominants contributions are the uniform SST increase (Figure 9b) and the CO_2 increase (Figure 9d). The former is almost entirely responsible for the tropospheric warming, including the tropical high-tropospheric amplification, and also substantially explains the low-tropospheric Arctic amplification (Figure 9b). The correlation coefficient between the total and the uniform SST warming responses is 0.81. The latter (CO_2 effect) cools the stratosphere and is responsible for only a weak warming of the troposphere (Figure 9b), which corresponds to the theoretical expectation (Vallis et al, 2015; Shine et al, 2003). The temperature response to the Arctic sea ice loss is a warming in the near-surface high latitudes — it dominates the Arctic surface warming — but remains strictly confined to this area (Figure 9c). The SST pattern change is responsible for a weak but significant warming in the tropical troposphere and a cooling of the troposphere north of 30°North (Figure 9e). At the surface it corresponds to a generalized cooling of the Northern extratropics, especially in the North Atlantic (not shown). This regional-seasonal cooling is compensated in others regions and seasons so that the global-annual mean temperature response to the SST pattern anomaly is close to zero, which is expected by construction.

5.2 Zonal wind response

Zonal-mean zonal wind changes associated with temperature changes described in the previous paragraph are presented in Figure 10. The main effect is again the uniform SST warming which almost entirely explains the strengthening of the zonal wind at around 30°N (Figure 10b). It is also associated with a weakening of the polar vortex which is counter-balanced by both CO_2 and SST pattern effects (Figure 10d,e). These changes are consistent with Figure 9 and the thermal wind balance. A poleward shift of the zonal wind is also identified in the mid-to-low troposphere for this particular season, consistent with Figure 7a. The SST pattern also induces a slight strengthening and southward shift of the tropospheric jet stream (Figure 10e) which moderates the poleward shift near the surface induced by the uniform SST increase (Figure 10b). We find that within the CFMIP protocol and according to CNRM-CM6-1, the Arctic sea ice loss has no significant impact on the zonal wind (Figure 10c). This somewhat conflicts previous studies based on coupled simulations (including the CNRM-CM5 model) which identified a southward shift of the eddy-driven jet in response to Arctic sea ice loss (Deser et al, 2015; Oudar et al, 2017; McCusker et al, 2017; Screen et al, 2018). A reason for that is that here, the Arctic amplification induced by the sole Arctic sea ice loss remains strictly confined to the surface and does not modify the meridional temperature gradient above 700 hPa (Figure 9c).

Focusing now on the lower-tropospheric circulation, Figure 11 shows the decomposition of the 850 hPa zonal wind response to an abrupt increase of CO_2. The total response obtained in the AGCM model is shown on panel a. It exhibits a poleward shift over all the Northern Hemisphere. The dominant contribution is again the uniform SST warming which explains most aspects of the total response (correlation coefficient of 0.76). It is not surprising since the uniform SST experiment captures the main changes in the meridional temperature gradient, i.e. the amplified warming in both tropical upper-troposphere and Arctic lower-troposphere. The main difference is that the northward shift of the zonal wind in the Atlantic extend more longitudinally in the uniform SST warming than in the total response. Note that the squeezing of the zonal wind is also visible in OND (Figures 10a and 11a), but to a lesser extent compared to JFM, and is mostly explained by the uniform SST warming, consistent with Harvey et al (2015). Potential drivers have been identified by Zappa and Shepherd (2017) and correspond to the Arctic amplification, the tropical amplification and the variability of the stratospheric vortex. It appears that the sea ice loss and the CO_2 effects have almost no significant impact (Figure 11c,d), even if the sign of their contribution corresponds to what is theoretically expected: the response to CO_2 projects onto a poleward jet shift whereas the response to Arctic sea ice loss resembles a southward shift, especially in the Atlantic. The response to the SST pattern change (Figure 11e) is somewhat anti-correlated to the uniform SST increase effect, since this experiment simulates a generalized cooling of the boreal winter extratropics. Only in the Pacific, the change in SST pattern acts to reinforce the response to the uniform SST warming, suggesting that changes in SST gradients amplify the strengthening of the jet observed over this area.

5.3 Origins of the dynamical changes: Eady Growth Rate

To better understand the dynamical changes, we analyze the eady growth rate (EGR) response (Lindzen and Farrell (1980), also used in Graff and LaCasce (2012); Yin (2005); Oudar et al (2017)), which is a measure of baroclinicity in the atmosphere (Figure 12).

In the total response (Figure 12a), the EGR increases near the surface in the mid and high latitudes, increases in the tropical high-troposphere and decreases in the mid-latitudes mid-troposphere. This can be directly related to the change in the zonal-mean temperature (Figure 9a): the warming of the tropical high-troposphere enhances the meridional temperature gradient thus the EGR increases in the high-troposphere at 30°N. Oppositely, the warming in the Arctic low-troposphere reduces the meridional temperature gradient and thus the EGR decreases. The warming near the surface, especially in the Arctic, is responsible for a decrease of the vertical temperature gradient and of the static stability. This leads to an increase of baroclinicity. The structure observed is consistent with Oudar et al (2017) who showed the changes in EGR at the end of the 21st century in the CNRM-CM5 model following the RCP8.5 scenario.

Consistently with previous figures, the total response is mostly explained by the uniform SST warming (Figure 12b). The pattern observed is close to the total response, except in the polar stratosphere where the EGR decreases, in agreement with the increase in temperature (Figure 9b) and the decrease in zonal wind (Figure 10b). This polar stratospheric decrease in EGR obtained in the uniform SST experiment is counter-balanced, in the total response, by both CO_2 and SST pattern contributions (Figure 12d,e). Elsewhere, the EGR response to CO_2 is relatively weak and exhibits only few significant changes consistent with a weak poleward shift of the zonal wind while the pattern SST induces a weak southward shift of the mid-tropospheric baroclinicity, in line with previous figures.

6 Discussion

The main purpose of this paper is to investigate the boreal winter (ONDJFM) atmospheric circulation response to an abrupt increase of CO_2 in the new CNRM-CM6-1 model. First of all, care must be taken in generalizing the results found in this study to other models. It has been shown that the atmospheric circulation change exhibits various response to CO_2 in CMIP5 models (Barnes and Polvani, 2015; Peings et al, 2018; Zappa and Shepherd, 2017) and while one model displays a northward shift of the zonal wind, another one could display a southward shift. Thus, it is necessary to examine the atmospheric circulation response in other CMIP6 models when more of them will be available.

Our results suggest that the uniform SST warming is the major contributor to changes in the mid-latitude dynamics. The changes observed are explained by modification in the meridional temperature gradient as highlighted by the Eady growth rate response. However, we have also highlighted that robust changes in the mid-latitude dynamics are difficult to assess due to the strong internal variability. Signal-to-noise ratio is particularly weak in the Atlantic for ONDJFM and JFM seasons, but not for OND season. In the Pacific, conclusions are rather different and robust responses are found for any seasons. Previous studies (Barnes and Polvani, 2013; Woollings et al, 2010) have defined the eddy-driven jet position as the maximum zonal wind over the domain 60W-0;15N-75N, we here show the importance of defining a maximum zonal wind position in other regions.

Another important feature that can influence changes in the jet position is the role of clouds. In Section 5, we have seen that the uniform SST warming is the dominant effect in the response to an abrupt increase of CO_2. Several studies have gone one step further in this decomposition and have suggested that changes in atmospheric cloud radiative effect may explain a substantial part of the poleward shift of the mid-latitude eddy-driven jet seen in uniform SST increase experiments (Ceppi and Hartmann, 2016; Ceppi and Shepherd, 2017; Voigt and Shaw, 2016; Li et al, 2019). Panels f in Figures 9, 10, 11 and 12 shows the cloud radiative feedback for the near-surface temperature, the 850 hPa zonal wind, the zonal-mean temperature, the zonal-mean zonal wind and the EGR respectively (see Section 2 and Table 1 for details). In general, the effect of clouds is weak and not significant for OND season. Concerning the 850 hPa zonal wind, clouds cause a northward shift (Figure 11f) but no significance is found, except a weakening over the south-west of both the Atlantic. The increase detected on the northern side of the maximum climatology is however not significant. For the zonal-mean fields, significance is mostly found in the tropical high-troposphere, which is not the main focus of this paper. Lastly, concerning the EGR response (Figure 12f), we notice a poleward shift of baroclinicity near the surface but again no significance is found. The influence of clouds have also been investigated in other seasons, but no significant response has been found (not shown), except in the annual mean in which a weak but significant poleward shift is observed in the lower troposphere (Figure 13). This results is consistent with previous studies (Voigt et al (2019) among others).

7 Conclusion

In this study, we have analyzed the wintertime Northern Hemisphere mid-latitude atmospheric circulation response to a quadrupling of CO_2 in the CNRM-CM6-1 global climate model. We have evaluated the model by comparing it to the previous version CNRM-CM5. In general, the representation of mid-latitude atmospheric circulation has been improved in CNRM-CM6-1 although the zonal bias — which is common to climate models — remains present. The response to an increase of CO_2 has been investigated in the coupled model and in atmosphere-only simulations, that allows for breaking the total response into individual contribution of CO_2, SST and sea-ice changes. Our main findings can be summarized as follows:

1. The general response of the mid-latitude dynamics to an increase in CO_2 is a poleward shift of the westerly flow (including the eddy-driven jet), at the exception of the JFM season over the Atlantic region for which a squeezing of the flow is observed. Internal variability is strong in the Atlantic especially for ONDJFM and JFM seasons in which many years of simulations are needed to obtain significance.
2. The uniform SST warming is the dominant factor to explain atmospheric circulation changes and is mainly responsible for the squeezing of the variability found over Northern Europe. It exhibits maximum warming near the surface in polar regions (part of the Arctic amplification) and in the tropical upper-troposphere, implying a decrease of the meridional temperature gradient in the low-troposphere (decrease of baroclinicity) and an increase of the meridional temperature gradient in the upper-troposphere (increase of baroclinicity). This

results in an upward shift of the upper-level jet stream and a slight poleward shift of the 850 hPa westerly flow.

3. The direct radiative effect of CO_2 exhibits weak and not significant anomalies in the dynamics. However, CO_2 leads to significant cooling of the stratosphere and, to a lesser extent, warming of the troposphere. On the zonal-mean it seems that CO_2 is responsible for a weak poleward shift of the eddy-driven jet, consistent with Grise and Polvani (2014).
4. The Arctic sea ice loss effect is also weak and not significant. The induced warming remains strictly confined to the polar atmosphere near the surface, and therefore only weakly contributes to the Arctic amplification. It is associated with a decrease of the baroclinicity in the low-level mid-latitudes and an increase of baroclinicity over the polar region near the surface. The smaller sea ice loss effect on mid-latitude circulation compared with previous works (Deser et al, 2015, among others) might be due to the protocol which is based on atmosphere-only simulations (rather than coupled). However, this result contrasts with the one found by Harvey et al (2015). Using the HadGAM1 atmospheric model, they concluded that polar amplification is associated with a significant equatorward shift of the 850 hPa zonal wind and a decrease storminess in winter. Thus, the response to the Arctic sea ice loss in AMIP models can be model-dependent.
5. The response to the change in SST pattern is relatively weak and exhibits a southward shift in the Atlantic and a strengthening over the eastern Pacific. Note that the response to the SST pattern is characterized by a cooling of the North Atlantic, similar to the warming hole identified in both observations (Rahmstorf et al, 2015; Drijfhout et al, 2012) and global climate models (Gervais et al, 2018, 2019). In particular, Gervais et al (2019) found that it was responsible for significant changes in the baroclinicity. Thus, it would be interested to investigate the dynamical response to the SST pattern in more details, and it could be the subject of a future dynamical study.

6. The effects of clouds is relatively weak in CNRM-CM6-1 and no poleward shift is found in winter. However, the poleward shift of the jet is enhanced in the annual mean in response to the cloud radiative effects. This result is consistent with previous studies who suggested an enhancement of the poleward jet shift due to the cloud radiative feedback.

Finally, a result that appears to be robust is the squeezing of the variability over Western Europe. Consequently, an increase of extratropical storms is expected over Europe and could have societal impacts (Woollings et al, 2012). The increase of storminess has been highlighted in previous studies based on CMIP5 models (Ulbrich et al, 2008; Zappa et al, 2013). The main drivers of the zonal wind variability over Europe have been identified by Zappa and Shepherd (2017) and are the Arctic amplification, the tropical amplification and the variability of the stratospheric vortex. However, one could think of other drivers, as for example the North Atlantic warming hole or the teleconnection with tropical regions. This result gives the opportunity to investigate more the dynamical response over that specific region, looking at storm-track and others diagnostics.

Acknowledgments

The work described in this paper has received funding from the European Union's Horizon 2020 Research and Innovation program under grant agreement No 727862. We thank the CNRM-CM modeling team and in particular Aurore Voldoire for running the experiments of CNRM-CM6-1. The authors thank Aurélien Ribes for discussion of the results.

References

Barnes EA, Polvani L (2013) Response of the midlatitude jets, and of their variability, to increased greenhouse gases in the cmip5 models. Journal of Climate 26(18):7117–7135

Barnes EA, Polvani LM (2015) Cmip5 projections of arctic amplification, of the north american/north atlantic circulation, and of their relationship. Journal of Climate 28(13):5254–5271

Barnes EA, Simpson IR (2017) Seasonal sensitivity of the northern hemisphere jet streams to arctic temperatures on subseasonal time scales. Journal of climate 30(24):10,117–10,137

Bony S, Stevens B, Frierson DM, Jakob C, Kageyama M, Pincus R, Shepherd TG, Sherwood SC, Siebesma AP, Sobel AH, et al (2015) Clouds, circulation and climate sensitivity. Nature Geoscience 8(4):261

Brayshaw DJ, Hoskins B, Blackburn M (2008) The storm-track response to idealized sst perturbations in an aquaplanet gcm. Journal of the Atmospheric Sciences 65(9):2842–2860

Cattiaux J, Cassou C (2013) Opposite CMIP3/CMIP5 trends in the wintertime Northern Annular Mode explained by combined local sea ice and remote tropical influences. Geophys Res Lett 40(14):3682–3687, DOI 10.1002/grl.50643

Cattiaux J, Peings Y, Saint-Martin D, Trou-Kechout N, Vavrus SJ (2016) Sinuosity of midlatitude atmospheric flow in a warming world. Geophysical Research Letters 43(15):8259–8268

Ceppi P, Hartmann DL (2015) Connections between clouds, radiation, and midlatitude dynamics: A review. Current Climate Change Reports 1(2):94–102

Ceppi P, Hartmann DL (2016) Clouds and the atmospheric circulation response to warming. Journal of Climate 29(2):783–799

Ceppi P, Shepherd TG (2017) Contributions of climate feedbacks to changes in atmospheric circulation. Journal of Climate 30(22):9097–9118

Ceppi P, Zelinka MD, Hartmann DL (2014) The response of the southern hemispheric eddy-driven jet to future changes in shortwave radiation in cmip5. Geophysical Research Letters 41(9):3244–3250

Ceppi P, Zappa G, Shepherd TG, Gregory JM (2018) Fast and slow components of the extratropical atmospheric circulation response to co2 forcing. Journal of

Climate 31(3):1091–1105

Chadwick R, Douville H, Skinner CB (2017) Timeslice experiments for understanding regional climate projections: Applications to the tropical hydrological cycle and european winter circulation. Climate dynamics 49(9-10):3011–3029

Chang EK, Guo Y, Xia X (2012) Cmip5 multimodel ensemble projection of storm track change under global warming. Journal of Geophysical Research: Atmospheres 117(D23)

Chevallier M, Salas y Mélia D, Voldoire A, Déqué M, Garric G (2013) Seasonal forecasts of the pan-arctic sea ice extent using a gcm-based seasonal prediction system. Journal of Climate 26(16):6092–6104

Craig A, Valcke S, Coquart L (2017) Development and performance of a new version of the oasis coupler, oasis3-mct_3. 0. Geoscientific Model Development 10(9):3297–3308

Decharme B, Delire C, Minvielle M, Colin J, Vergnes JP, Alias A, Saint-Martin D, Séférian R, Sénési S, Voldoire A (2018) Recent changes in the isba-ctrip land surface system for use in the cnrm-cm6 climate model and in global off-line hydrological applications. Journal of Advances in Modeling Earth Systems

Dee DP, Uppala S, Simmons A, Berrisford P, Poli P, Kobayashi S, Andrae U, Balmaseda M, Balsamo G, Bauer dP, et al (2011) The era-interim reanalysis: Configuration and performance of the data assimilation system. Quarterly Journal of the royal meteorological society 137(656):553–597

Deser C, Phillips AS (2009) Atmospheric circulation trends, 1950–2000: The relative roles of sea surface temperature forcing and direct atmospheric radiative forcing. Journal of Climate 22(2):396–413

Deser C, Tomas RA, Sun L (2015) The role of ocean–atmosphere coupling in the zonal-mean atmospheric response to arctic sea ice loss. Journal of Climate 28(6):2168–2186

Drijfhout S, Van Oldenborgh GJ, Cimatoribus A (2012) Is a decline of amoc causing the warming hole above the north atlantic in observed and modeled warming patterns? Journal of Climate 25(24):8373–8379

Eyring V, Bony S, Meehl GA, Senior CA, Stevens B, Stouffer RJ, Taylor KE (2016) Overview of the coupled model intercomparison project phase 6 (cmip6) experimental design and organization. Geoscientific Model Development (Online) 9(LLNL-JRNL-736881)

Francis JA, Vavrus SJ (2012) Evidence linking arctic amplification to extreme weather in mid-latitudes. Geophysical Research Letters 39(6)

Gervais M, Shaman J, Kushnir Y (2018) Mechanisms governing the development of the north atlantic warming hole in the cesm-le future climate simulations. Journal of Climate 31(15):5927–5946

Gervais M, Shaman J, Kushnir Y (2019) Impacts of the north atlantic warming hole in future climate projections: Mean atmospheric circulation and the north atlantic jet. Journal of Climate 32(10):2673–2689

Graff LS, LaCasce J (2012) Changes in the extratropical storm tracks in response to changes in sst in an agcm. Journal of Climate 25(6):1854–1870

Grise KM, Polvani LM (2014) The response of midlatitude jets to increased co2: Distinguishing the roles of sea surface temperature and direct radiative forcing. Geophysical Research Letters 41(19):6863–6871

Harvey B, Shaffrey L, Woollings T (2014) Equator-to-pole temperature differences and the extra-tropical storm track responses of the cmip5 climate models. Climate dynamics 43(5-6):1171–1182

Harvey B, Shaffrey L, Woollings T (2015) Deconstructing the climate change response of the northern hemisphere wintertime storm tracks. Climate dynamics 45(9-10):2847–2860

Holland MM, Bitz CM (2003) Polar amplification of climate change in coupled models. Climate Dynamics 21(3-4):221–232

Kushner PJ, Held IM, Delworth TL (2001) Southern hemisphere atmospheric circulation response to global warming. Journal of Climate 14(10):2238–2249

Li Y, Thompson DW, Bony S, Merlis TM (2019) Thermodynamic control on the poleward shift of the extratropical jet in climate change simulations: The role of rising high clouds and their radiative effects. Journal of Climate 32(3):917–934

Lindzen R, Farrell B (1980) A simple approximate result for the maximum growth rate of baroclinic instabilities. Journal of the atmospheric sciences 37(7):1648–1654

Madec G, Bourdallé-Badie R, Bouttier P, Bricaud C, Bruciaferri D, Calvert D, et al (2017) Nemo ocean engine. https://zenodo org/record/1472492#XGNEUc83kUE

Manzini E, Karpechko AY, Kornblueh L (2018) Nonlinear response of the stratosphere and the north atlantic-european climate to global warming. Geophysical Research Letters 45(9):4255–4263

McCusker KE, Kushner PJ, Fyfe JC, Sigmond M, Kharin VV, Bitz CM (2017) Remarkable separability of circulation response to arctic sea ice loss and greenhouse gas forcing. Geophysical Research Letters 44(15):7955–7964

Meehl GA, Stocker TF, Collins WD, Friedlingstein P, Gaye AT, Gregory JM, Kitoh A, Knutti R, Murphy JM, Noda A, et al (2007) Global climate projections. climate change 2007: the physical science basis. contribution of working group i to the fourth assessment report of the intergovernmental panel on climate change

Oudar T, Sanchez-Gomez E, Chauvin F, Cattiaux J, Terray L, Cassou C (2017) Respective roles of direct ghg radiative forcing and induced arctic sea ice loss on the northern hemisphere atmospheric circulation. Climate dynamics 49(11-12):3693–3713

Peings Y, Cattiaux J, Vavrus SJ, Magnusdottir G (2018) Projected squeezing of the wintertime north-atlantic jet. Environmental Research Letters 13(7):074,016

Rahmstorf S, Box JE, Feulner G, Mann ME, Robinson A, Rutherford S, Schaffernicht EJ (2015) Exceptional twentieth-century slowdown in atlantic ocean overturning circulation. Nature climate change 5(5):475

Santer BD, Thorne P, Haimberger L, Taylor KE, Wigley T, Lanzante J, Solomon S, Free M, Gleckler PJ, Jones P, et al (2008) Consistency of modelled and observed temperature trends in the tropical troposphere. International Journal of Climatology 28(13):1703–1722

Scheff J, Frierson DM (2012) Robust future precipitation declines in cmip5 largely reflect the poleward expansion of model subtropical dry zones. Geophysical Research Letters 39(18)

Screen JA, Simmonds I (2010) The central role of diminishing sea ice in recent arctic temperature amplification. Nature 464(7293):1334

Screen JA, Deser C, Smith DM, Zhang X, Blackport R, Kushner PJ, Oudar T, McCusker KE, Sun L (2018) Consistency and discrepancy in the atmospheric response to arctic sea-ice loss across climate models. Nature Geoscience 11(3):155

Seidel DJ, Fu Q, Randel WJ, Reichler TJ (2008) Widening of the tropical belt in a changing climate. Nature geoscience 1(1):21

Shine KP, Bourqui M, Forster PdF, Hare S, Langematz U, Braesicke P, Grewe V, Ponater M, Schnadt C, Smith C, et al (2003) A comparison of model-simulated trends in stratospheric temperatures. Quarterly Journal of the Royal Meteorological Society 129(590):1565–1588

Simmonds I, Lim EP (2009) Biases in the calculation of southern hemisphere mean baroclinic eddy growth rate. Geophysical Research Letters 36(1)

Simpson IR, Shaw TA, Seager R (2014) A diagnosis of the seasonally and longitudinally varying midlatitude circulation response to global warming. Journal of the Atmospheric Sciences 71(7):2489–2515

Staten PW, Rutz JJ, Reichler T, Lu J (2012) Breaking down the tropospheric circulation response by forcing. Climate dynamics 39(9-10):2361–2375

Ulbrich U, Pinto JG, Kupfer H, Leckebusch G, Spangehl T, Reyers M (2008) Changing northern hemisphere storm tracks in an ensemble of ipcc climate change simulations. Journal of climate 21(8):1669–1679

Vallis GK, Zurita-Gotor P, Cairns C, Kidston J (2015) Response of the large-scale structure of the atmosphere to global warming. Quarterly Journal of the Royal Meteorological Society 141(690):1479–1501

Voigt A, Shaw TA (2016) Impact of regional atmospheric cloud radiative changes on shifts of the extratropical jet stream in response to global warming. Journal of Climate 29(23):8399–8421

Voigt A, Albern N, Papavasileiou G (2019) The atmospheric pathway of the cloud-radiative impact on the circulation response to global warming: important and uncertain. Journal of Climate 32(10):3051–3067

Voldoire A, Sanchez-Gomez E, y Mélia DS, Decharme B, Cassou C, Sénési S, Valcke S, Beau I, Alias A, Chevallier M, et al (2013) The cnrm-cm5. 1 global climate model: description and basic evaluation. Climate Dynamics 40(9-10):2091–2121

Voldoire A, Saint-Martin D, Sénési S, Decharme B, Alias A, Chevallier M, Colin J, Guérémy JF, Michou M, Moine MP, et al (2019) Evaluation of cmip6 deck experiments with cnrm-cm6-1. Journal of Advances in Modeling Earth Systems

Webb MJ, Andrews T, Bodas-Salcedo A, Bony S, Bretherton CS, Chadwick R, Chepfer H, Douville H, Good P, Kay JE, et al (2017) The cloud feedback model intercomparison project (cfmip) contribution to cmip6. Geoscientific Model Development 2017:359–384

Woollings T, Hannachi A, Hoskins B (2010) Variability of the north atlantic eddy-driven jet stream. Quarterly Journal of the Royal Meteorological Society 136(649):856–868

Woollings T, Gregory JM, Pinto JG, Reyers M, Brayshaw DJ (2012) Response of the north atlantic storm track to climate change shaped by ocean–atmosphere coupling. Nature Geoscience 5(5):313

Woollings T, Barnes E, Hoskins B, Kwon YO, Lee RW, Li C, Madonna E, McGraw M, Parker T, Rodrigues R, et al (2018) Daily to decadal modulation of jet variability. Journal of Climate 31(4):1297–1314

Yin JH (2005) A consistent poleward shift of the storm tracks in simulations of 21st century climate. Geophysical Research Letters 32(18)

Zappa G, Shepherd TG (2017) Storylines of atmospheric circulation change for european regional climate impact assessment. Journal of Climate 30(16):6561–6577

Zappa G, Shaffrey LC, Hodges KI, Sansom PG, Stephenson DB (2013) A multi-model assessment of future projections of north atlantic and european extratropical cyclones in the cmip5 climate models. Journal of Climate 26(16):5846–5862

Zappa G, Hoskins BJ, Shepherd TG (2015) Improving climate change detection through optimal seasonal averaging: The case of the north atlantic jet and european precipitation. Journal of Climate 28(16):6381–6397

List of Tables

Table 1 CNRM-CM6-1 experiments used in this study. The Δ used in the `piSST-pxK` experiment is applied uniformly and corresponds to the difference in global mean SST between `abrupt-4xCO2` and `piControl` experiments.

Sec.	Abb.	Name	SST forcing	Sea ice forcing	CO_2 forcing	LW CRE	Length
3	-	historical	*(coupled)*	*(coupled)*	obs.	x	10×36 yr
	-	amip	obs.	obs.	obs.	x	36 yr
4	CPI	piControl	*(coupled)*	*(coupled)*	pre-industrial	x	1500 yr
	C4C	abrupt-4xCO2	*(coupled)*	*(coupled)*	quadrupled	x	1500 yr
5	API	piSST	piControl	piControl	pre-industrial	x	390 yr
	ACO2	piSST-4xCO2	piControl	piControl	quadrupled	x	30 yr
	AUNI	piSST-pxK	piControl + Δ	piControl	pre-industrial	x	30 yr
	ASST	a4SST	abrupt-4xCO2	piControl	pre-industrial	x	30 yr
	AICE	a4SSTice	abrupt-4xCO2	abrupt-4xCO2	pre-industrial	x	30 yr
	A4C	a4SSTice-4xCO2	abrupt-4xCO2	abrupt-4xCO2	quadrupled	x	390 yr
5-6	-	amip	obs.	obs.	obs.	x	36 yr
	-	amip-p4k	obs. + 4 K	obs.	obs.	x	36 yr
	-	amip-lwoff	obs.	obs.	obs.		36 yr
	-	amip-p4k-lwoff	obs. + 4 K	obs.	obs.		36 yr

List of Figures

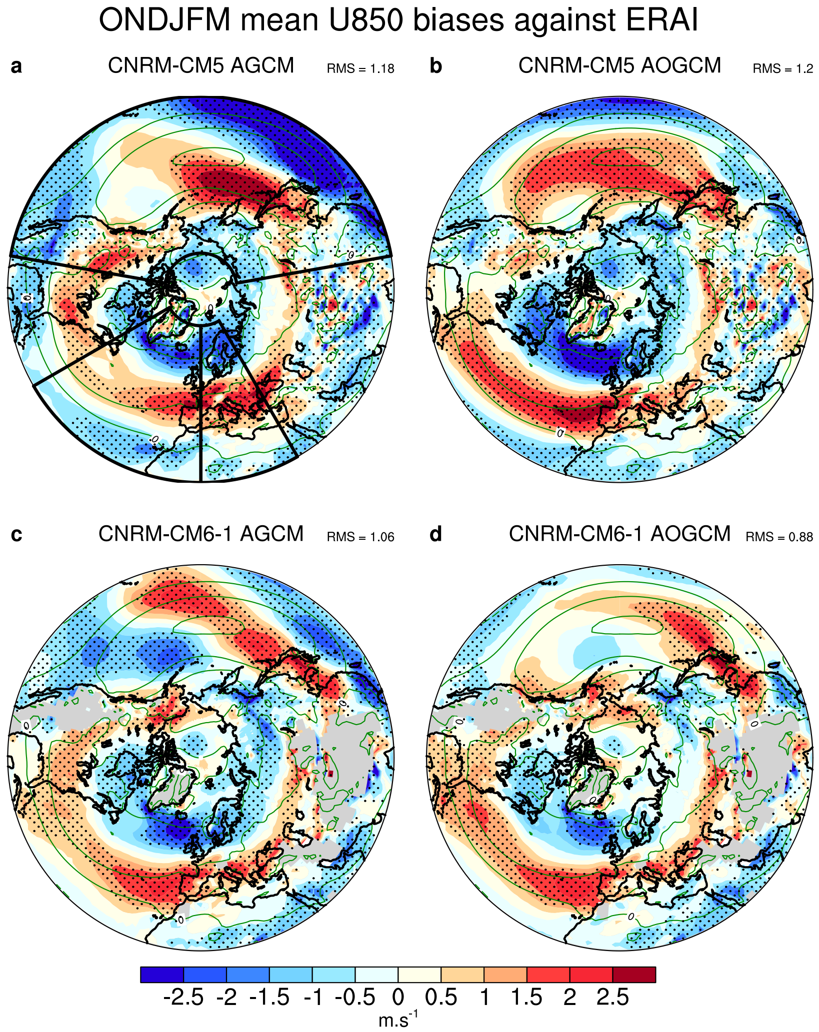

Fig. 1 Biases of zonal wind at 850 hPa (m/s) in ONDJFM for (a) CNRM-CM5.1 AGCM version, (b) CNRM-CM5.1 AOGCM version, (c) CNRM-CM6-1 AGCM version and (d) CNRM-CM6-1 AOGCM version. Biases are estimated as the difference between the historical ensemble mean averaged over 1979-2014 and ERAI reanalysis over the same period. Note that the rcp8.5 is used to extend the historical experiment of CNRM-CM5.1 (AOGCM mode). The green contours indicate the climatology computed using ERAI (contour interval is $5 m.s^{-1}$). Stippling indicates differences that are significant at the 95% confidence level. The root mean square (RMS) is indicated on the top right of each panel. The black lines indicate the three regions defined in Section 2.3.

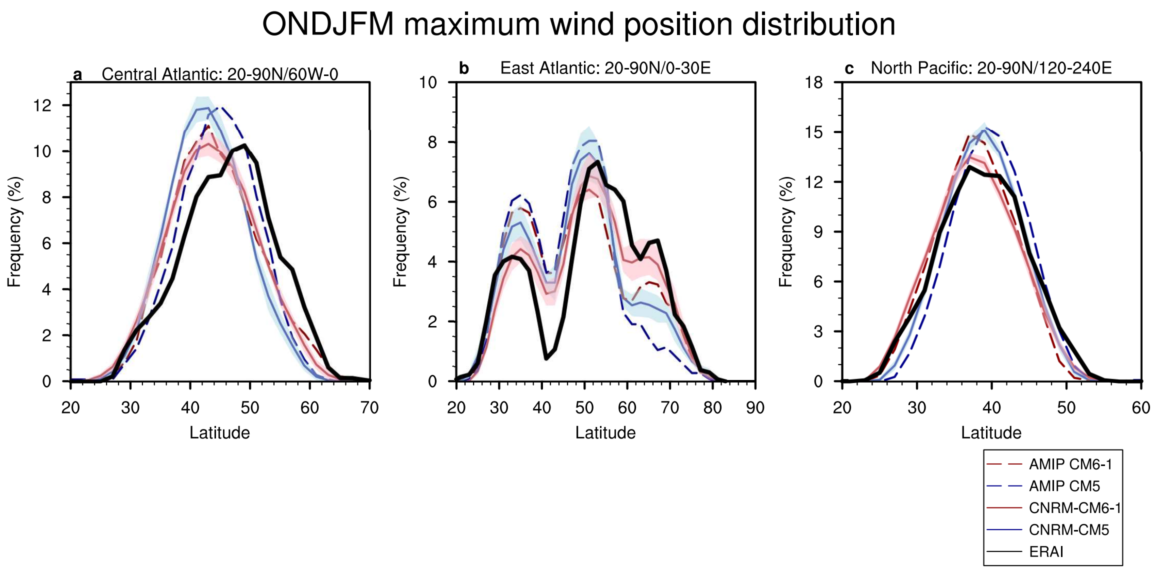

Fig. 2 Frequency of occurrence of the maximum wind position position in ERAI (black line), CNRM-CM5 (blue line) and CNRM-CM6 (red line) for (a) the central Atlantic domain (20-90N/60W-0), (b) the east Atlantic domain (20-90N/0-30E) and (c) the Pacific domain (20-90N/120-240E). Historical simulations are used for CNRM-CM5 and CNRM-CM6-1 over the 1979-2014 period. Note that in the case of CNRM-CM5, the rcp8.5 has been used to extend the historical simulation which ends in 2005. The blue and red shadings correspond to the standard deviation across the historical ensemble members.

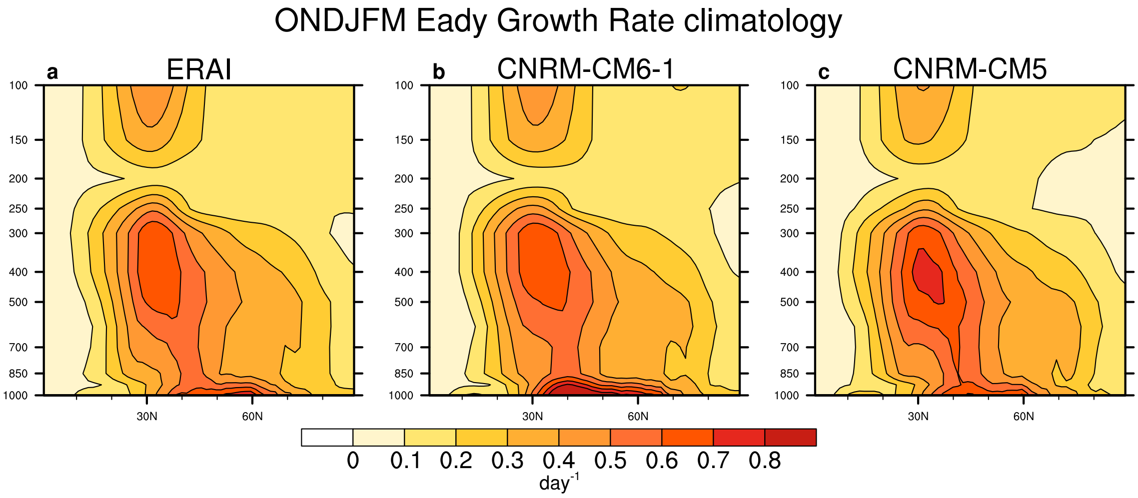

Fig. 3 Climatology of the Eady growth rate for (a) ERA-Interim, (b) CNRM-CM6-1 historical experiment and (c) CNRM-CM5 historical experiment (in day^{-1}. The climatologies are computed over the common period 1979-2014.

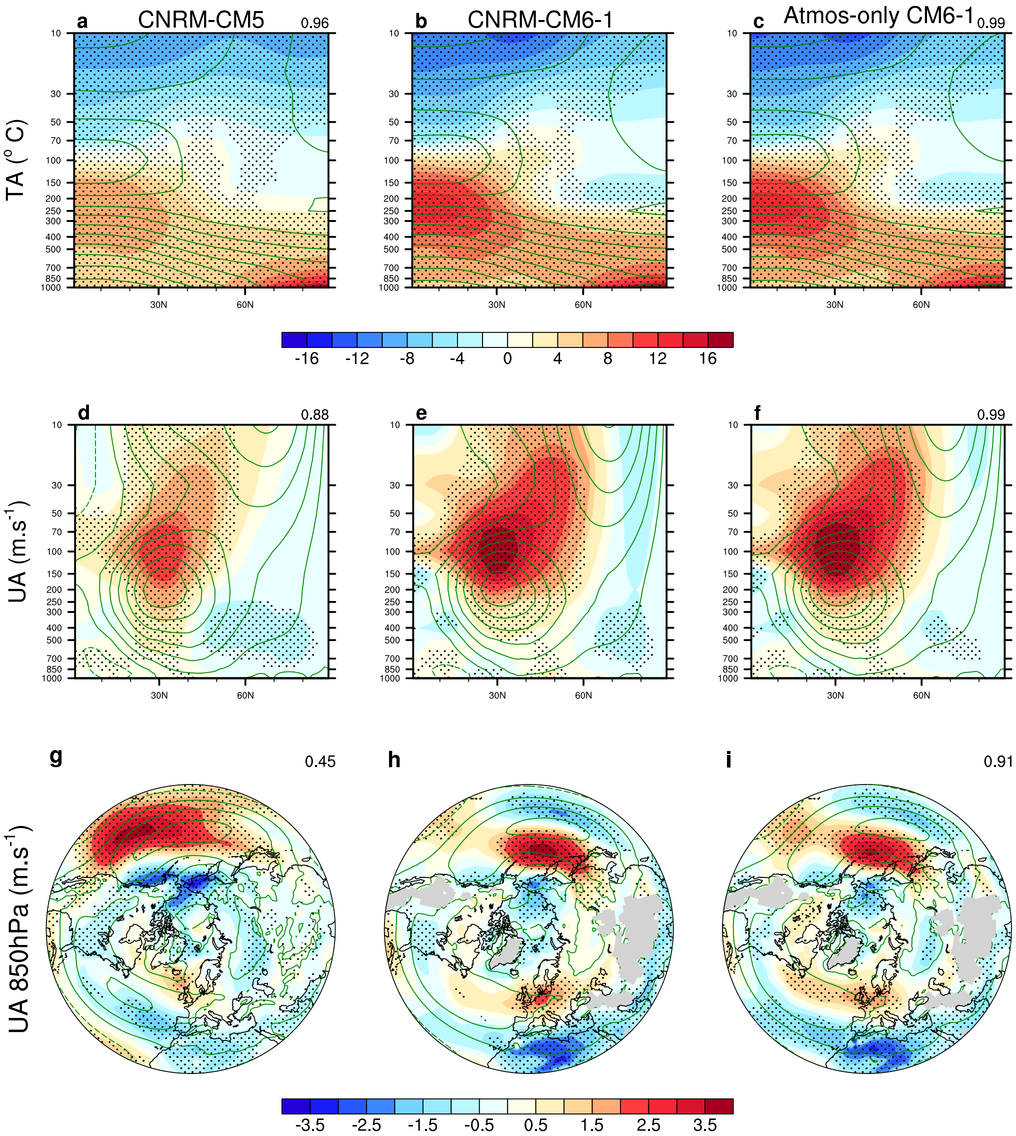

Fig. 4 (a),(b),(c) Zonal-mean temperature response in ONDJFM for CNRM-CM5, CNRM-CM6-1 and atmosphere-only CM6-1 respectively. (d),(e),(f) Zonal-mean zonal wind response. (g),(h),(i) 850 hPa zonal wind response. The green contours correspond to the climatological mean computed in the control simulation of each model (contour intervals are 10 K, 5 m.s^{-1} and 5 m.s^{-1} for the temperature, zonal wind and 850 hPa zonal wind respectively). Stipplings indicate responses that are significant at the 95% confidence level. The correlation between each panel and CNRM-CM6-1 (middle panel) is indicated on the top right.

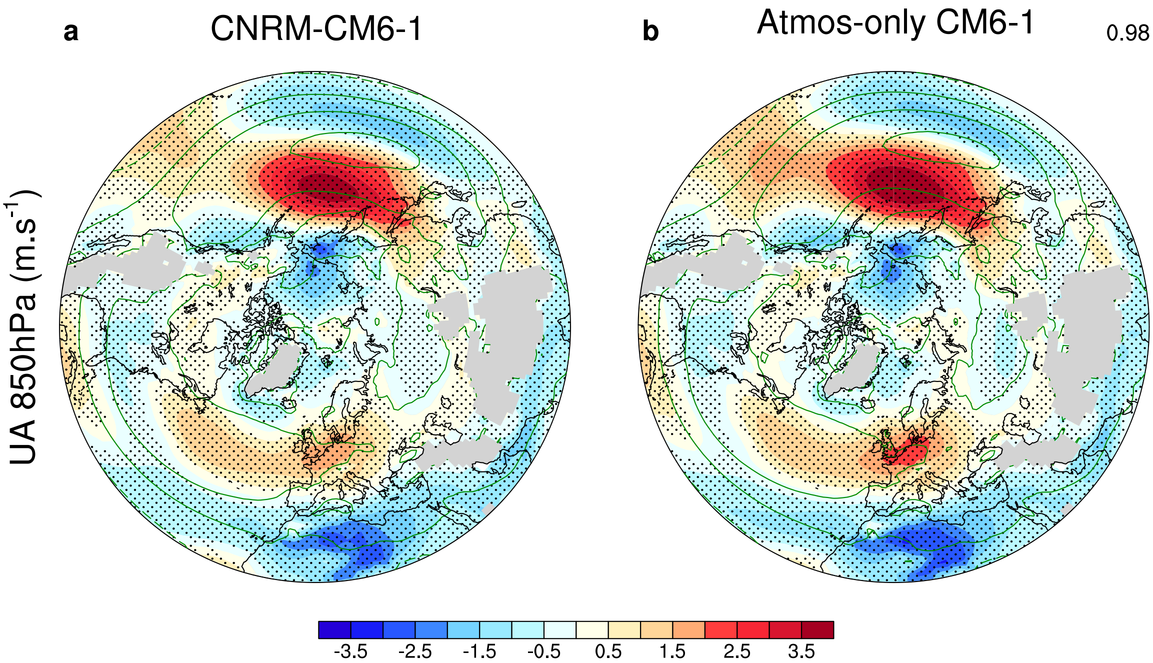

Fig. 5 850 hPa zonal wind response in ONDJFM for (a) CNRM-CM6-1 and (b) atmosphere-only CM6-1 when using all years available (390 in total for the AGCM experiments). The green contours correspond to the climatological mean computed in the control simulation of each model (contour intervals are 5 m.s^{-1}). Stipplings indicate responses that are significant at the 95% confidence level. The correlation between the two panels is indicated on the top right.

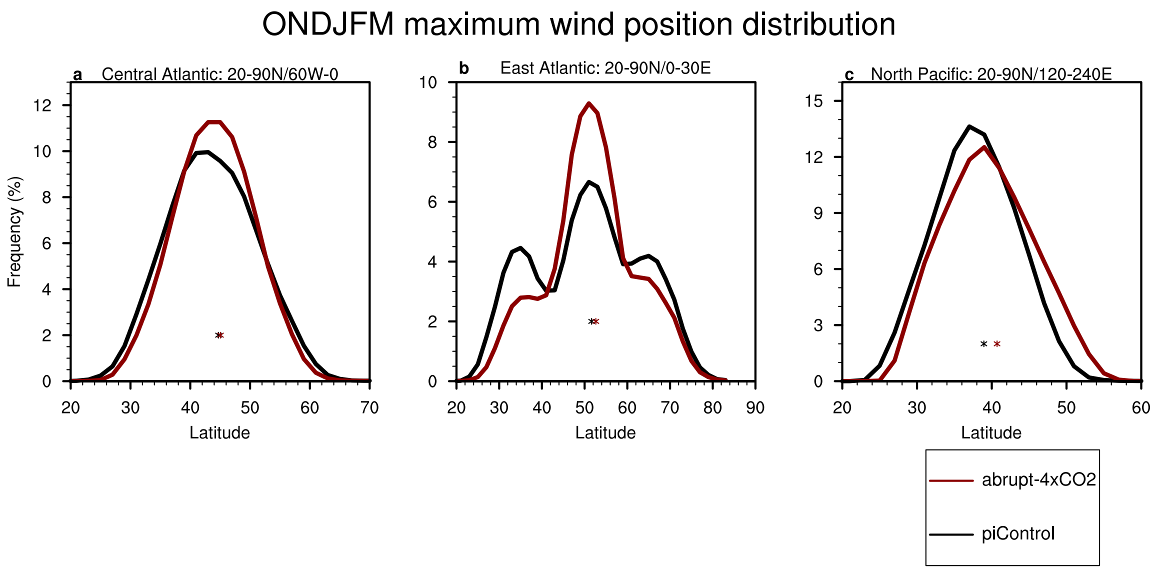

Fig. 6 Probability distribution function (PDF) of the maximum wind position of the piControl simulation (in black) and the abrupt-4xCO2 simulation (in red) for (a) the central Atlantic domain (20-90N/60W-0), (b) the east Atlantic domain (20-90N/0-30E) and (c) the Pacific (20-90N/120-240E). The PDF is computed over all years available for both simulations, after removing the first 110 years. The two asterisks correspond to the mean maximum wind position.

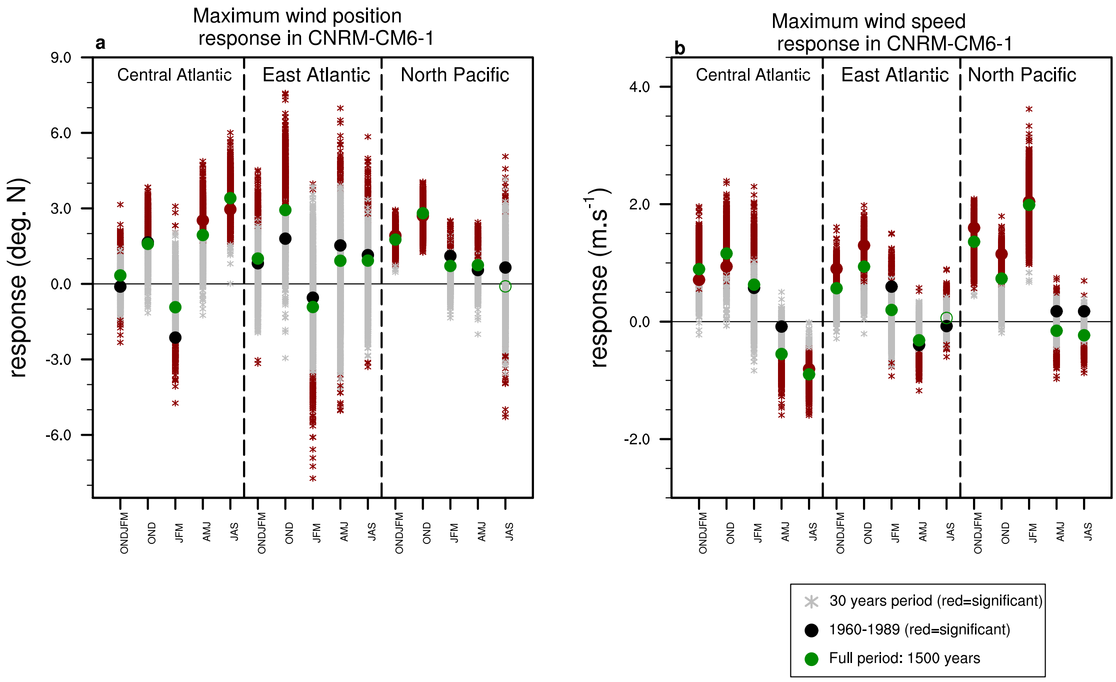

Fig. 7 Scatter plot of (a) the maximum wind position and (b) the speed responses in CNRM-CM6-1 (abrupt-4xCO2 - piControl) for the Central Atlantic, East Atlantic and North Pacific domains and for ONDJFM, OND, JFM, AMJ and JAS seasons. The responses are computed over the full period (1500 years, green circle filled if significants), the 1960-1989 period (black (red) dots (if significant)), and 1000 samples of 30 years selected randomly in the 1500 years (gray (red) cross (if significant at the 95% confidence level)).

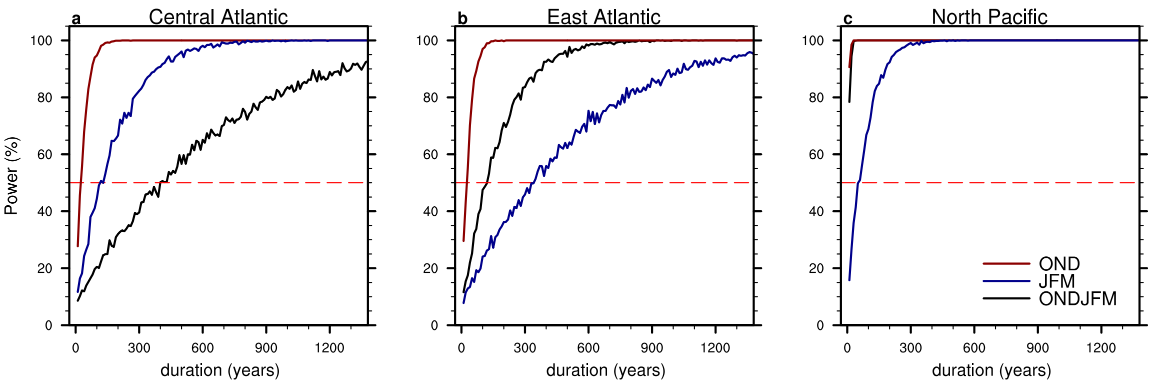

Fig. 8 Time series of the robustness of the maximum wind position response between the abrupt-4xCO2 and piControl simulations in function of the duration of the simulation for (a) the central Atlantic domain (20-90N/60W-0), (b) the east Atlantic domain (20-90N/0-30E) and (c) the Pacific (20-90N/120-240E), in black for ONDJFM, in blue for JFM and in red for OND. For each N from 10 to 1500, we randomly select 1000 samples of N years in the 1500 years available for both CPI and C4C simulations and calculate the C4C minus CPI mean difference over each sample. For each duration, we count the number of times when the response is of the same sign of the response found over the full period and significant at the 95% confidence level. The dashed red line indicate when robustness is found (50%).

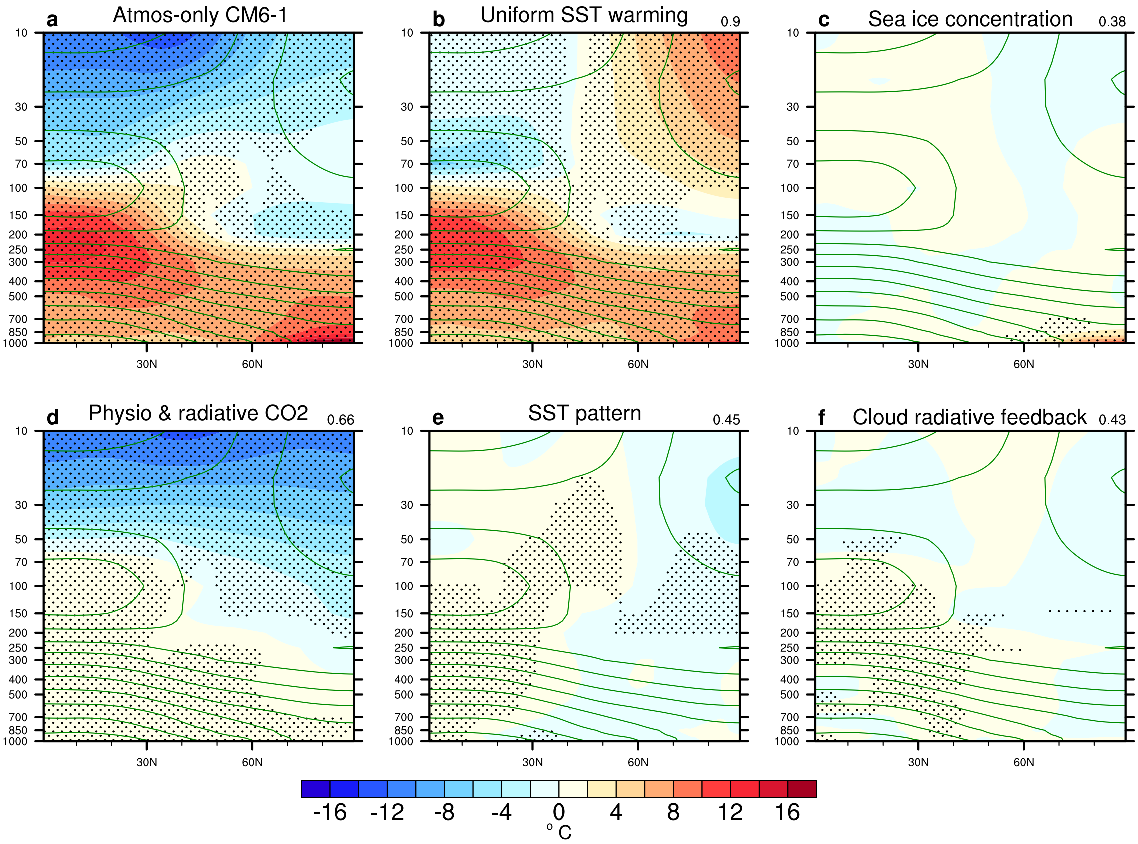

Fig. 9 Zonal-mean temperature response in OND for (a) Atmosphere-only CM6-1, (b) the uniform SST warming, (c) sea ice concentration, (d) physiological and radiative CO_2, (e) SST pattern and (f) the cloud radiative feedback. The green contours correspond to the climatology computed in the control simulation piSST (contour interval is 10K). Stipplings indicate responses that are significant at the 95% confidence level. Correlations between panel a (total response) and each effect is indicated on the top right.

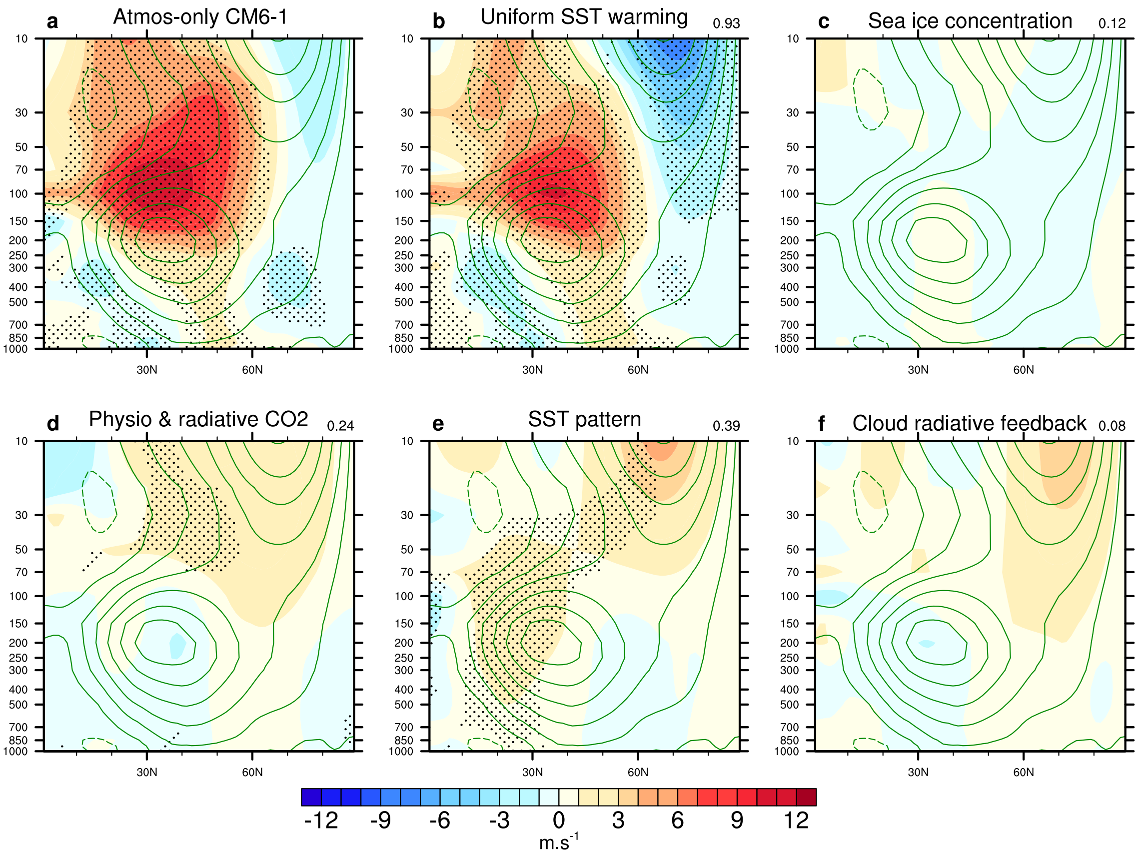

Fig. 10 Same as Figure 9 but for the zonal-mean zonal wind (contour interval is 5 m.s^{-1} for the climatology).

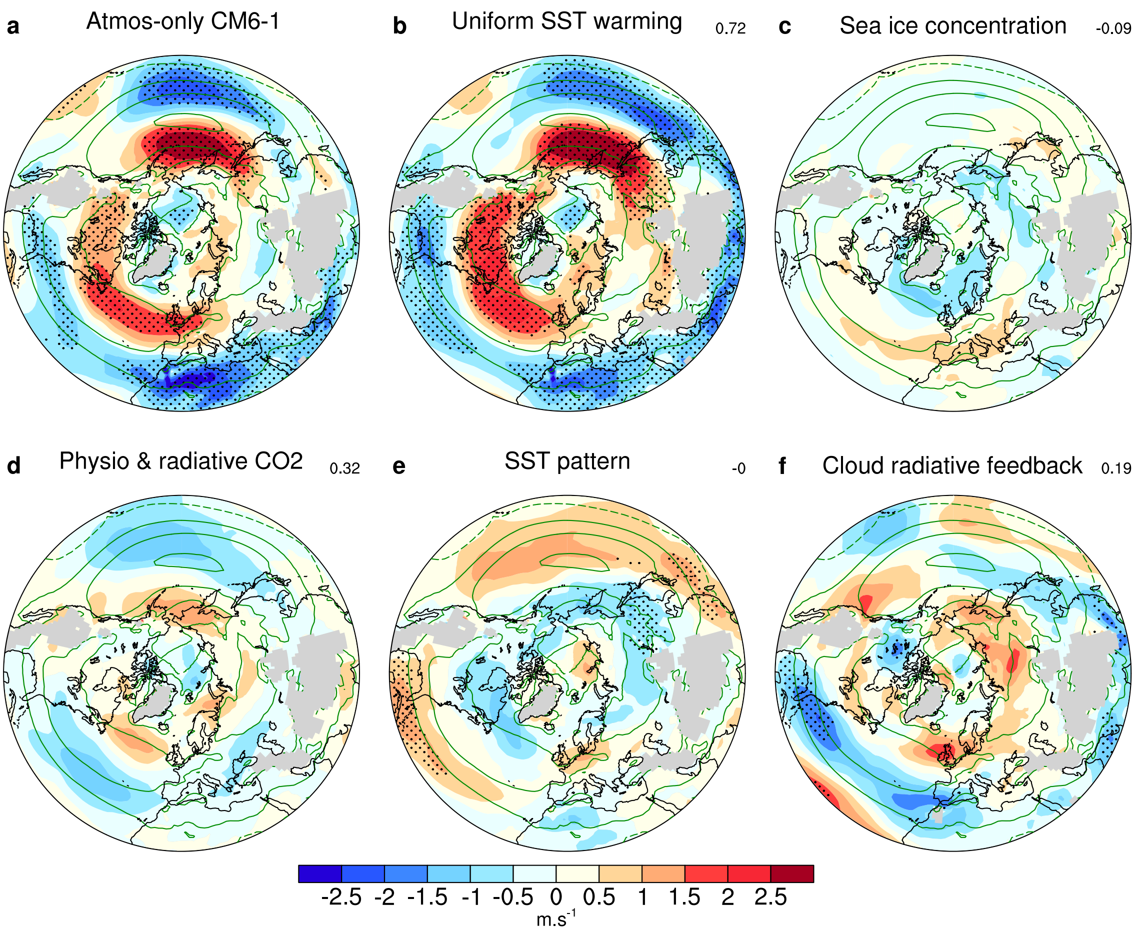

Fig. 11 Same as Figure 9 but for the 850 hPa zonal wind (contour interval is 5 m.s^{-1} for the climatology).

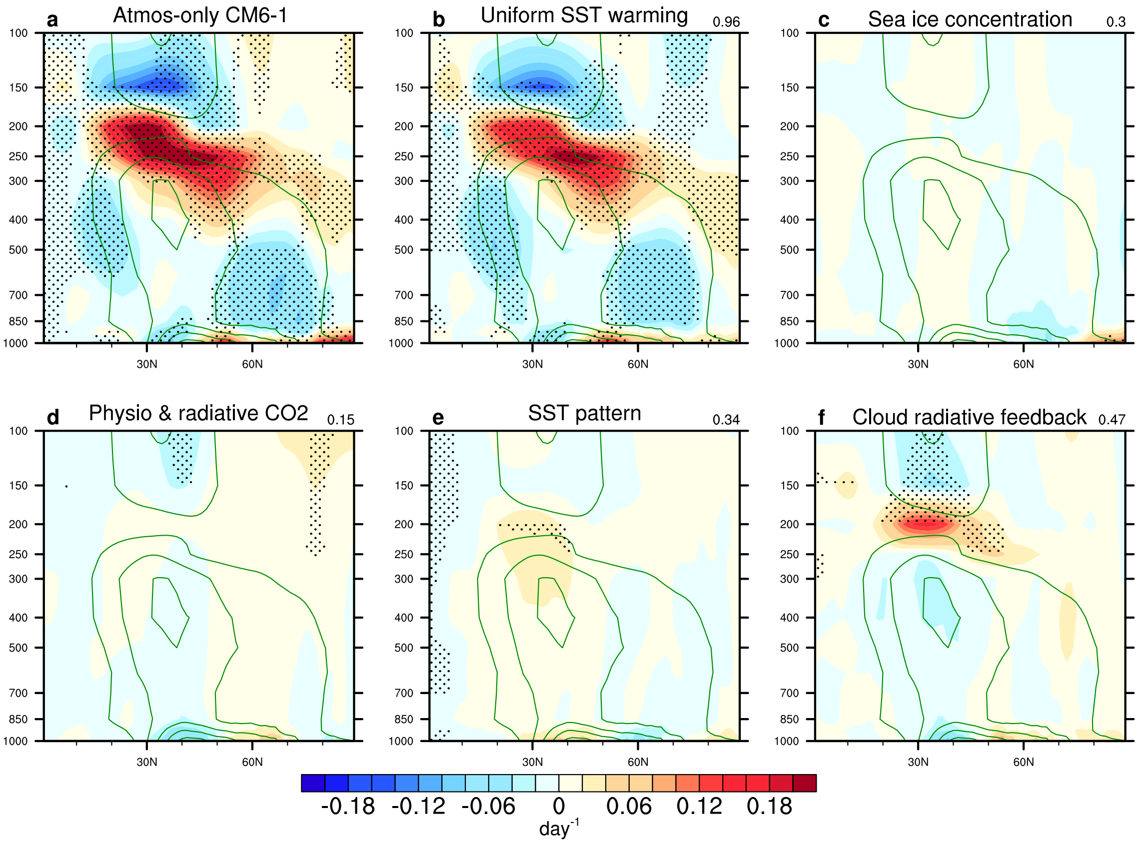

Fig. 12 Same as Figure 9 but for the zonal-mean Eady Growth Rate (contour interval is 0.2 day^{-1} for the climatology).

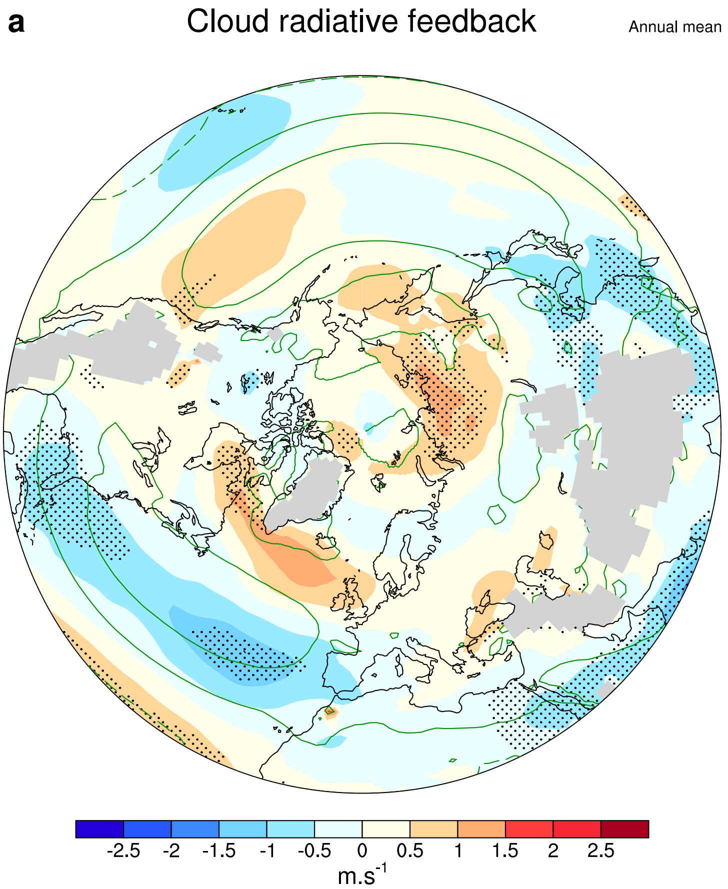

Fig. 13 Annual mean 850 hPa zonal wind response for the cloud radiative effect.